Materials Chemistry and Physics 306 (2023) 128023

Contents lists available at ScienceDirect

Materials Chemistry and Physics

journal homepage: www.elsevier.com/locate/matchemphys

Differences in HF Wet Etching Resistance of PECVD SiN_x:H thin films

Matteo Barcellona [a], Orazio Samperi [a], Davide Russo [a], Anna Battaglia [b], Dirk Fischer [c], Maria Elena Fragalà [a,*]

[a] Dipartimento di Scienze Chimiche and INSTM UdR Catania, Università degli Studi di Catania, Viale Andrea Doria 6, 95127, Catania, Italy
[b] Lam Research SRL, Viale Colleoni 11, 20864, Agrate Brianza, MB, Italy
[c] Lam Research GmbH, Manfred-von-Ardenne-Ring 20, Haus A, 01099, Dresden, Germany

HIGHLIGHTS

- Wet etching behavior in HF solution of PECVD thin films not linearly correlated to hydrogen concentration.
- Differences between Si-H and N-H bond densities are indicative of a different acid corrosion resistivity.
- Role of oxygen impurities on etching behavior, especially at the highest HF concentration.
- Similar film composition and comparable WER after annealing.
- A straightforward and simple procedure to measure film thickness by FT-IR data is provided.

GRAPHICAL ABSTRACT

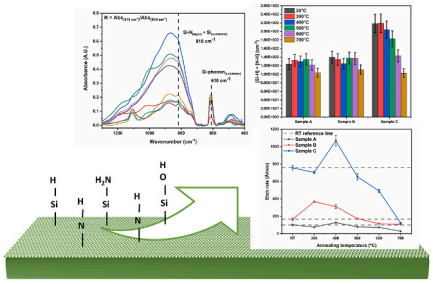

ABSTRACT

Hydrogenated silicon nitride (SiNx:H) thin films are deposited by plasma-enhanced chemical vapor deposition (PECVD) using different gas mixtures of SiH_4+NH_3+N_2 or SiH_4+N_2 and plasmas conditions. Resulting differences in terms of overall film composition are herein associated with wet etch rate (WER) in hydrofluoric acid (HF). Different acid concentrations, as well as etching temperatures, have been investigated and it is demonstrated that not only hydrogen but also the oxygen content of nitride have a strong impact on film chemical resistivity. The role of annealing of nitride layers is also studied in terms of wet etching response and further elucidates the role of crystalline structure and chemical evolution of oxidized components on HF nucleophilic attack mechanism. Samples have been characterized by Field Emission-Scanning Electron Microscopy (FE-SEM), X-rays Photoelectron Spectroscopy (XPS), Fourier Transform Infrared Spectroscopy (FT-IR), and X-Ray Diffraction (XRD). The WER is measured by implementing a fast and straightforward FT-IR data treatment.

1. Introduction

Si_3N_4 has found application in a plethora of fields, from orthodontics, and metallurgy to the realization of parts for the aviation, energy, and mechanical industries. The Si_3N_4 is suitable in semiconductor device manufacturing as a passivation sacrificial layer [1–3], hard mask [4], implantation spacers [5,6], for the realization of optoelectronic/CMOS devices [7,8], and various other applications.

The recent interest in high electron mobility transistors (HEMTs) based on III-V compounds requires the use of silicon nitride dielectrics at the AlGaN/GaN interfaces to minimize 2 DEG electron capture in AlGaN causing DC-to-RF current dispersion [9–11]. The thin film of Si_3N_4 deposited by CVD is extremely useful as a passivation layer in electronic devices due to the higher relative dielectric constant (ε = 6–9) as compared to the values measured for silica films [12]. In the semiconductor industry, a broad range of deposition recipes to deposit silicon

* Corresponding author.
E-mail address: me.fragala@unict.it (M.E. Fragalà).

https://doi.org/10.1016/j.matchemphys.2023.128023
Received 16 February 2023; Received in revised form 25 May 2023; Accepted 1 June 2023
Available online 5 June 2023

nitride films is available, depending on several deposition methods used for different applications, such as CVD [13,14], PECVD [14,15], LPCVD [14,15], APCVD [16,17]. Among them, LPCVD uses high deposition temperature and results in almost stoichiometric Si_3N_4, whereas PECVD operates at a lower temperature (~400 °C) using a plasma source, thus resulting in higher N/Si ratios, lower film densities, and higher hydrogen content than LPCVD deposited films [15,18]. PECVD is the most commonly used method to deposit low-temperature silicon nitride for HEMTs: typical gases used as precursors for silicon nitride depositions are SiH_4, NH_3, and N_2 and, accordingly, by varying precursor gases' composition and flowing speeds as well as plasma conditions, films with different characteristics are obtained. However, the process suffers the drawback of a relatively high concentration of hydrogen in the samples that is associated with low-density films and has an adverse role on device performances.

Herein we investigate the role of film composition on the wet etch rate of the nitride layer in hydrofluoric acid (HF) solutions at different concentrations and temperatures [19]. SiN_x:H layers, deposited by Plasma Enhanced Chemical Vapor Deposition (PECVD), characterized by different hydrogen content, are etched in hydrofluoric acid solution (ranging from 0.5 wt% and 5 wt%) to study their wet etch rate (WER) in hydrofluoric acid (HF) solutions.

Obtained results point to a role of overall film composition on WER with a crucial role played by H content on selectivity while oxygen content results more important towards acid concentration. The effect of nitride annealing on etching behavior is also scrutinized.

2. Materials and methods

2.1. Si_3N_4 deposition

Hydrogenated silicon nitride (SiN_x:H) thin films are deposited on 200 mm silicon wafers by plasma-enhanced chemical vapor deposition (PECVD) using Lam Research VECTOR reactor. Capacity-coupled plasma is generated between two metal electrodes with dual plasma excitation frequencies. The main feature of this system is its flexibility with different RF operation modes. Typically, PECVD deposition is performed by applying 13.56 MHz High-Frequency RF (HF). Low-Frequency RF (LF) at 400 kHz can be used in combination with the HF RF to modulate film properties. In particular, film stress and film density can be optimized by using the right balance between HF and LF powers. This is obtained by modulating the ion bombardment with LF power. The characteristic operating power ranges from 100 to 500 W for HF and from 0 to 200 W for LF. The usual pressure range is between 2 and 6 Torr. Gas mixtures of $SiH_4 + NH_3 + N_2$ or $SiH_4 + N_2$ are commonly used and the composition of SiN films strongly depends on the gas mixture and plasmas conditions. Deposited samples for this work have been maintained at a deposition temperature of 380 °C under different RF operation modes (single frequency and dual frequency, for example). $N_2 + SiH_4$ gas mixture at a N_2/SiH_4 ratio of about 70 or a combination of $N_2 + SiH_4 + NH_3$ with NH_3/SiH_4 and N_2/SiH_4 gas flow ratios of about 4.5 and 70 was used for the present study.

2.2. HF etching experiments

Hydrofluoric acid (HF) solutions at different concentrations were realized starting from a stock solution 48–51 wt% (density = 1.16 g/cm^3 (20 °C); Mw = 20.01 g/mol; Sigma-Aldrich). Working solutions were made by dilution in a 10 mL Teflon beaker with ultrapure water (18.2 MΩ cm, TOC 1 pbm, PURELAB Flex 3 by Elga Veolia company). HF working solutions were prepared at 0.55, 2.19, and 5.44 wt% taking into account variation of density after dilution. Etching experiments were performed at 25 °C by submerging diced samples (surface area ~1 cm^2) with the silicon nitride thin layer upward to repress diffusion issues. The samples were etched after different times (seconds or minutes). Washing in DI water and N_2 flow drying followed by etching in HF solution. The working solution was frequently refreshed to avoid reaction byproduct interference. Characterization analyses were promptly accomplished before the formation of the native oxide layer.

2.3. Samples thermal annealing

Thermal annealing was performed in a Tersid Carbolite tubular furnace under a vacuum environment at a pressure of $1{\cdot}10^{-1}$ Torr. An inert atmosphere was induced by Ar gas injection at a flow of 300 sccm. Annealing experiments were conducted at a temperature of 200 °C, 400 °C, 500 °C, 600 °C, and 700 °C and a heating ramp of 40 °C/min. The annealing time was set at 30 min. The samples were left to cool before exposure to the atmospheric environment.

2.4. X-Ray Photoelectron Spectroscopy (XPS)

Elemental and chemical analyses were performed by XPS characterization technique. In particular, the analysis was executed with a PHI 5000 VersaProbe II at a 45 °C take-off angle relative to the surface sample holder. The X-Ray source was an Al-Kα (1486.6 eV) with a pass energy of 187.85 eV for the survey and 23.5 eV for the multi-acquisitions. The chamber base pressure was $1{\cdot}10^{-8}$ Pa. Spectra calibration was executed by fixing the adventitious carbon C1s signal at 285.0 eV. Peak intensity was obtained prior to Shirley's background removal following elemental percentage calculation according to the sensitivity factor reported in the scientific literature [20]. Deconvolutions were executed by XPSPeak 4.1 free software [21].

2.5. Fourier-Transform infrared spectroscopy (FT-IR)

Chemical groups and thin layer thickness measurements were performed via infrared spectroscopic absorption with a Jasco FT-IR 4600 spectrophotometer. Spectra were acquired in the range of 400–4000 cm^{-1} wavenumber with a resolution of 1 cm^{-1}. Samples of about 1 cm^2 were placed in the sample holder to entirely catch the source beam. Spectra measurements were obtained at room temperature.

The determination of the Si-H and N-H group concentration (bonds/cm^3) was estimated following Equation (1) (X = Si or N):

$$[X-H]\left(cm^{-3}\right) = \frac{Peak\ area}{\sigma_{X-H}(cm^2) \bullet layer\ thickness\ (cm)} \quad \text{Eq. 1}$$

The peak area is calculated from the absorbance spectra, σ is the cross-section of Si-H and N-H bonds having $7.4{\bullet}10^{-18}$ cm^2 and $5.3{\bullet}10^{-18}$ cm^2 values, respectively [22,23] and the layer thickness is determined as discussed in Appendix A.

2.6. Field-Emission scanning electron microscopy (FE-SEM)

The thin layer thickness measurements, within 10 nm, were also performed by FE-SEM. The instrumentation is a VP-Supra 550 FE-SEM (Zeiss) with an electron probe accelerating voltage of 15 kV. The samples were cut in half with a diamond tip to reveal a thin layer of fresh lateral surface. Sliced samples were placed in side-view via a dedicated sample holder. The measurements were in good accordance with other characterization techniques.

2.7. X-rays diffraction (XRD)

Structural characterization was performed using a Smartlab Rigaku diffractometer in grazing incident mode (0.5 °) operating at 45 kV and 200 mA equipped with a rotating anode of Cu Kα radiation.

3. Results

Investigated silicon nitride layers are characterized by different optical and mechanical properties (Table 1). PECVD SiN layers deposited

Table 1
Properties of investigated PECVD nitride and oxynitride samples. The refractive index was measured at 633 nm. No absorption is detected at the same wavelength.

Sample	Dep. T (°C)	Thickness (Å)	Refractive Index	Stress (MPa)	% H[a]
A	380	2190	2.052	370	12
B	380	2100	1.922	−90	19
C	380	1864	1.974	696	21
SiO_XN_y	400	2060	1.775	117	25

[a] H% is calculated by RBS-ERDA.

at 380 °C are all amorphous (as observed by XRD analysis) and hydrogenated as indicated by the H% ranging from 12% to 21%. Film stress was measured by wafer bow changes before and after the deposition of the silicon nitride layer. The thickness of the layers was measured by ellipsometry.

Properties of a silicon oxynitride (SiO_XN_y) layer deposited by PECVD are reported in Table 1 for comparison: as expected, the refractive index value is lower (RI ~ 1.7–1.8) than that of silicon nitride (RI ~ 2), due to the presence of the higher amount of oxygen.

The density of bonded hydrogen, attributed to Si-H and/or N-H groups, can be easily detected by FT-IR spectroscopy (Fig. 1): the Si-H stretching mode signal is at ~ 2180 cm^{-1} (Fig. 1 inset) while the N-H stretching mode appears at ~ 3300 cm^{-1}. Si-N stretching mode is located between 870 cm^{-1} and 820 cm^{-1}. The formation of a thin layer of silicon dioxide or silicon oxynitride at the SiN/Si interface is responsible for the peak at 1100 cm^{-1} detected in the FT-IR spectra, while the peak at 610 cm^{-1} is related to the silicon substrate. FT-IR spectrum of the SiO_XN_y layer is shown for comparison to highlight the differences with the investigated silicon nitride layers. In particular, the broadening of the main Si-N peak is a result of the combination of Si-N and Si-*O*-Si bonding in the oxynitride layer.

An estimation of the density of N-H and Si-H bonds in the silicon nitride as-deposited samples, obtained by FT-IR analysis, is reported in Table 2.

The estimated densities are in good agreement with literature data [24]: to note, sample B shows a N-H bond density higher than Si-H whilst in both sample A and sample C the Si-H bond density is similar to that of N-H (See Table 2). To note, high N-H bond density is associated with compressive stress (Table 1) [25].

XPS analysis, reported in Table 3, indicates a sub-stoichiometric N/Si ratio for all the samples and, among them, sample B and sample C are the nitrogen and the silicon richest, respectively.

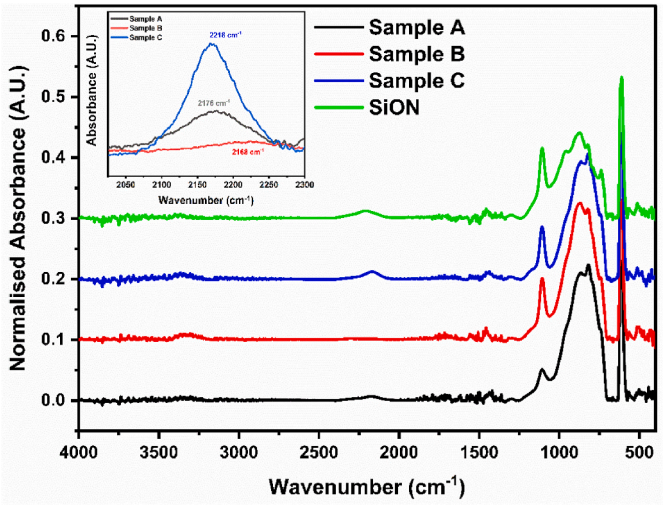

Fig. 1. FT-IR absorbance spectra of PECVD nitride and oxynitride layers. In the inset, the Si-H absorbance peaks of samples A, B, and C.

Table 2
N-H, Si-H and total bonded hydrogen density estimated from FT-IR analysis.

Sample	[Si-H] (bonds/cm^3)	[N-H] (bonds/cm^3)	[N-H] + [Si-H] (bonds/cm^3)
A	$6.38{\cdot}10^{21}$	$6.03{\cdot}10^{21}$	$1.24{\cdot}10^{22}$
B	$1.64{\cdot}10^{21}$	$1.24{\cdot}10^{22}$	$1.40{\cdot}10^{22}$
C	$1.17{\cdot}10^{22}$	$1.02{\cdot}10^{22}$	$2.19{\cdot}10^{22}$

Table 3
Surface atomic concentration of nitride and oxynitride layers determined by XPS.

Sample	C%	Si%	N%	O%	F%	N/Si	O/Si
A	12.87	30.92	28.32	27.89	NA	0.91	0.90
B	6.15	32.16	30.52	31.16	NA	0.95	0.97
C	11.57	31.34	23.73	33.35	NA	0.76	1.06
SiO_XN_y	14.68	28.83	9.36	47.13	NA	0.32	1.63

The high oxygen content at the silicon nitride surface is mainly due to surface oxidation, upon exposure to the atmosphere. SiO_XN_y surface composition is reported to highlight the differences with SiN_x:H layers in terms of N/Si and O/Si ratios. Such differences and intensity ratios remain almost unvaried (data not shown) after a short etch (60 s) in diluted HF 0.5 wt% solution. WER experiments are performed in unbuffered HF aqueous solutions, in a concentration range from 0.5 wt% up to 5 wt% (Table 4): layer thickness before and after etch has been measured by FT-IR following the procedure reported in Supplementary Material.

The wet etch rate is measured by varying etching time until the achievement of complete removal of the nitride layer (confirmed also by XPS analysis of the surface of the totally etched samples).

A linear relation between WER and HF concentration is observed for all the samples, but sample C is significantly more etchable than the other layers: the WER trend seems to confirm the role of H content in the chemical resistivity of silicon nitride, despite the behavior of sample C suggests other factors affecting the layer's HF etchability, especially at the higher HF concentration. To note, at [HF] > 0.5% the WER of sample C is about 4 times higher than that of sample B, despite the small difference in terms of H% measured by ERDA (see Table 1) and the comparable N-H bond density (see Table 2), generally directly related to HF etchability [26–28].

Annealing experiments, performed in a temperature range from 200 °C to 700 °C, show a slight decrease of the total H content for all the samples upon increasing annealing temperature, as expected at a temperature higher than deposition one. In particular, as reported in Fig. 2a, a more evident reduction of total H bonded density ([N-H + Si-H]) is observed above 600 °C for samples A and B, whilst sample C reveals this variation at T above 400 °C. Fig. 2b shows that WER in HF of annealed layer changes upon varying anneal temperature (Fig. 2b): in particular, we can observe an increase of WER up to 400 °C, while at a higher temperature, the WER reduction results in convergence of etching resistivity for all the three samples. After annealing at T = 700 °C the WER is almost the same for all the samples (Fig. 2b), in good agreement with the trend observed for the overall H content (Fig. 2a).

In order to elucidate this behavior, XPS analysis is performed on samples A and C (characterized by the lowest and the highest WER, respectively) after annealing at 400 °C and 700 °C: both samples feature

Table 4
Etch rate of silicon nitride samples of different HF solution concentrations.

Sample	HF 0.5 wt%	HF 2 wt%	HF 5 wt%
A	13 ± 2 Å/min	50 ± 5 Å/min	100 ± 9 Å/min
B	22 ± 2 Å/min	80 ± 5 Å/min	165 ± 14 Å/min
C	40 ± 1 Å/min	317 ± 18 Å/min	757 ± 25 Å/min

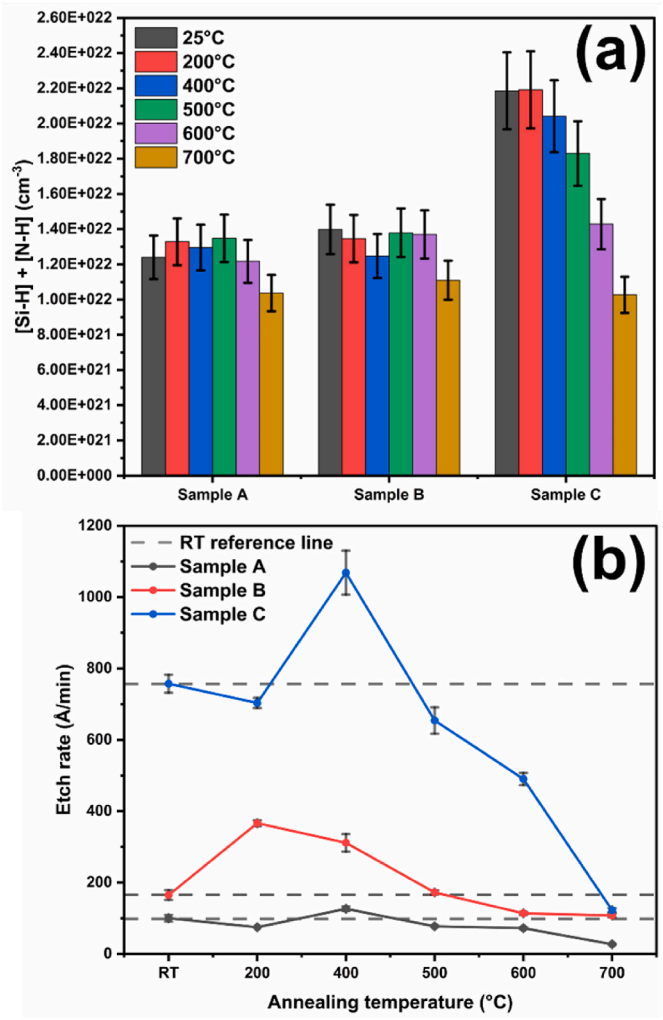

Fig. 2. a) Total Si-H and N-H group concentration of silicon nitride samples and b) WER in HF 5% before and after annealing. (For interpretation of the references to colour in this figure legend, the reader is referred to the Web version of this article.)

an increase of the N/Si ratio and a decrease of the O/Si ratio, which becomes almost comparable at 700 °C (Table 5).

To note, the oxygen content is attributed to contaminants incorporated in the nitride layer during deposition [29] and the presence of hydrogen in the nitride layer is responsible for its migration toward H-rich regions [30]. Accordingly, the formation of oxynitride-like regions within the layer can be assumed to influence the WER of the annealed sample.

Fig. 3 reports the Si2p photoelectron peak of sample A before (Fig. 3a) and after annealing at 400 °C (Fig. 3b) and 700 °C (Fig. 3c).

Different components can be identified and related to the presence of Si-O, Si-N, and Si-Si bonds. In particular, for the pristine sample (Fig. 3a) the main peak's component, attributed to Si-N bonds, is at 102.0 eV and the less intense one, at 103.6 eV, is associated with the SiO_2 presence [31,32]. After annealing at 400 °C, a peak narrowing can be observed (Fig. 3b) and the oxidized component is less intense and shifted at 103.3 eV. This shift points to the formation of an oxynitride having a SiO_3N stoichiometry [33,34], whilst the small component at 99.9 eV is attributed to elemental silicon due to the formation of silicon clusters [35]: this signal's evolution can represent an indication of an oxygen migration at the surface thus promoting, due to annealing, water evolution, and overall oxygen content's reduction. Therefore, with annealing, hydrogen desorption, and bond rearrangements occur in the material, probably composed of silicon-rich regions and nitrogen-rich regions.

Table 5
XPS N/Si and O/Si elemental ratio of samples A and C after annealing at 400 °C and 700 °C.

Sample	Anneal	O/Si	N/Si
A	25 °C	0.91	0.9
A	400 °C	0.39	1.22
A	700 °C	0.48	1.16
C	25 °C	1.06	0.76
C	400 °C	0.75	0.97
C	700 °C	0.59	1.03

Similarly, Fig. 4 shows the XPS Si2p photoelectron peak of sample C before (Fig. 4a) and after annealing at 400 °C (Fig. 4b) and 700 °C (Fig. 4c).

Differences with sample A are clearly visible: first of all, Si2p of the pristine sample (Fig. 4a) is characterized by three components centered at 99.9 eV, 101.6 eV, and 103.6 eV associated with Si-Si, Si-N, and Si-O bonds, respectively. The main component, associated with Si-N bonds, is centered to lower binding energy (101.6 eV) and the presence of the Si-Si component at 99.9 eV is well consistent with a N/Si ratio lower than that of sample A. After annealing at 400 °C (Fig. 4b) a new component at 102.2 eV associated with the formation of Si_3ON is observed [33]: however, at 700 °C this component is not detectable and the Si2p signal is comparable to the one recorded for sample A.

XRD analysis of samples annealed at 600 °C is aimed to define if amorphous to the crystalline phase transition is promoted by the compositional modification associated with observed hydrogen evolution: as shown in Fig. 5a, sample A and sample B remain amorphous whilst sample C (Fig. 5b) shows two peaks at $2\theta = 51.5°$ and $2\theta = 56.0°$, associated to (301) and (400)/(211) planes, respectively [36] that are indicative of the presence of α-Si_3N_4 small crystalline domains [37,38]. Accordingly, this increase in crystallinity comes with the enhancement of chemical resistance in HF solutions, associated with a decrease in WER value (Fig. 2b).

4. Discussion

WER of nitride samples deposited by using different PECVD recipes is studied by varying the HF from 0.5 wt% to 5 wt%. Thickness reduction during etching is evaluated by straightforward methodology allowing to use of FT-IR spectral analysis without suffering the silicon substrate contribution (see Supplementary Information).

Whatever the HF concentration, the WER of the nitride layer increases upon increasing the overall measured H content, but the WER of sample C is remarkably higher than that of samples A and B (Table 4). These WER differences are important in the perspective of selectivity adjustment in the silicon oxide and silicon nitride wet etching process [39,40].

WER of nitride mainly depends on hydrogen concentration [23,41] and experimental data support this hypothesis in terms of general WER trend. However, samples A and B, show a more similar etch resistivity in comparison with that of sample C: this finding can be better explained by referring to the bonded hydrogen density, estimated by FT-IR measurements (that considers the exclusive contribution of Si-H and N-H bonds) rather than to H% estimated by RBS-ERDA (that can be associated to hydrogen bonded to other contaminants in the layers, i.e. oxygen).

On the other hand, the WER increase observed for sample C upon varying HF concentration suggests a role played by difluoride species (H_2F_2 and HF_2^-) in film etching. In particular, as reported in the literature [28], the mechanism of etching of silicon nitride involves the formation of Si-F bonds by nucleophilic reaction with protonated Si-N-H groups, mainly regarding monofluoride (F^-) species. At the same time, if Si-OH groups are present, their reaction with HF solution follows a

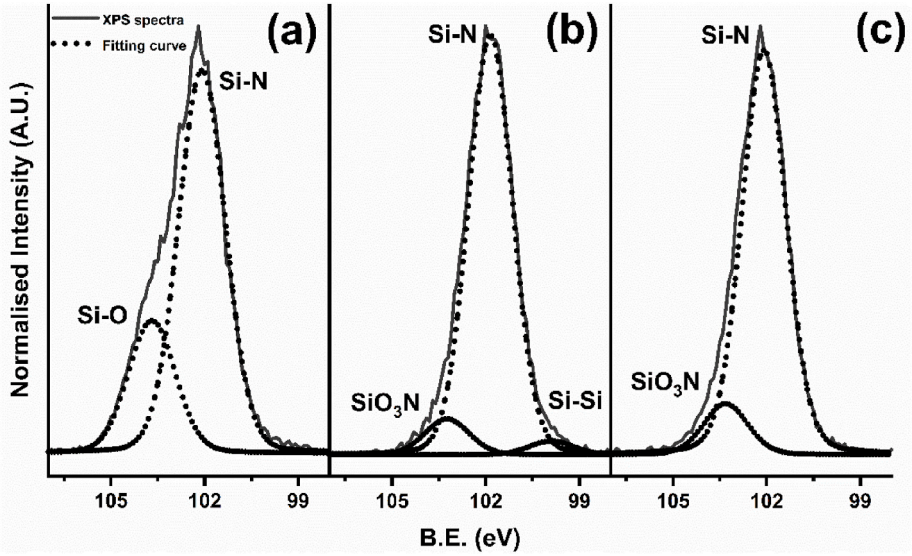

Fig. 3. Sample A XPS Si2p signal of (a) pristine; (b) annealed 400 °C 30min; and (c) annealed 700 °C 30min.

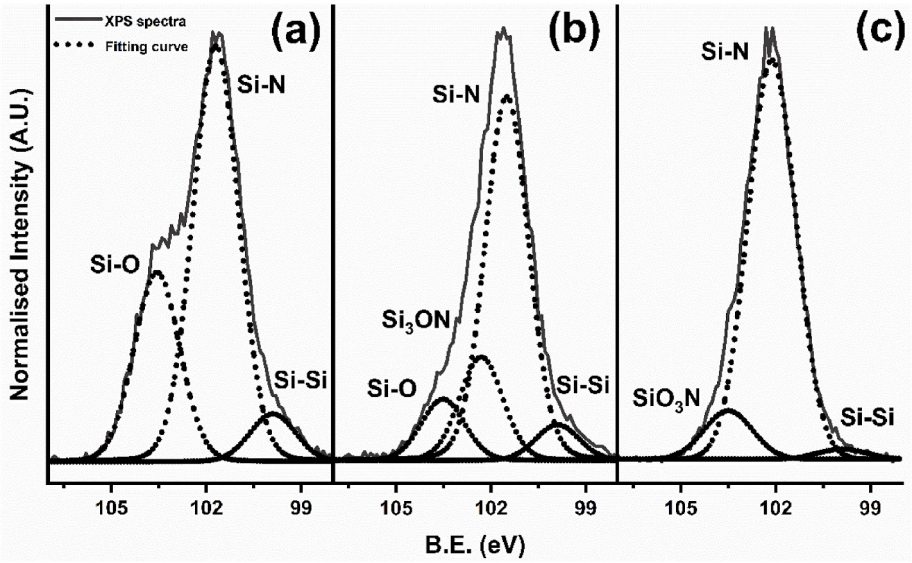

Fig. 4. Sample C XPS Si2p signal: (a) pristine; (b) annealed 400 °C 30min; and (c) annealed 700 °C 30min.

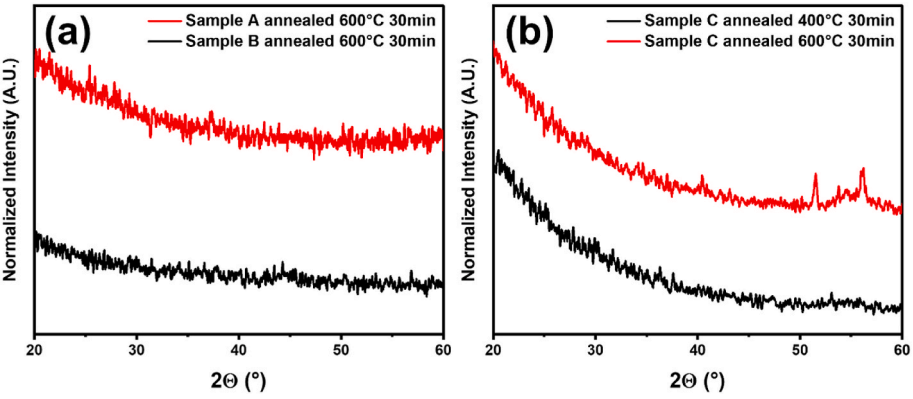

Fig. 5. XRD diffraction pattern of (a) sample A and sample B at 600 °C thermal annealing for 30 min and (b) sample C at 400 °C and 600 °C thermal annealing for 30 min.

different mechanism: in fact, the dissolution of silicon dioxide in aqueous HF-based solutions depends not only on pH but also on fluorinated charged and neutral species present in solutions (mainly HF_2^- and H_2F_2) that govern both protonations of silanol groups and nucleophilic attack to silicon center [26].

The behavior of sample C can be, hence, associated not only with the highest hydrogen content but also with the highest O/Si ratio responsible for the presence of Si-OH groups, more responsive to concentrate HF etching: in fact, incorporated oxygen in the nitride network promotes a more pronounced reactivity towards difluoride nucleophiles formed upon increasing the HF concentration [40,42,43].

In addition, investigated layers are characterized by different N/Si ratios: we can assume that the presence of Si-H bonds is associated with an increase in the etch rate of amorphous silicon nitride layers deposited by PECVD. In fact, if from a chemical point of view, Si-NH groups are responsible for nucleophilic attack of fluoride ions, -Si-H groups can be responsible for a different density of the layer [32]. The obtained results, thus suggest how the presence of both N–H and Si–H species in the nitride layer contributes effectively to the increase of the etching rate [38]: in particular, the low density of Si-H groups in sample B is indicative of a higher density of Si-N bonds (in good agreement with XPS data) that need to be broken to release SiF_4 during wet etch. Accordingly, the WER decrease is not linearly related to the overall H% (detected by ERDA and FT-IR). Such an explanation agrees well also with data related to annealed samples, whose WER converge at 700 °C together with the overall film composition expressed in term of N/Si and O/Si ratios (Table 5).

On the other hand, the role played by oxygen content, reasonably due to well-known contamination during the silicon nitride PECVD process, to trigger the WER in HF solution is corroborated by the peculiar behavior of sample C observed by XPS: in particular, moderate annealing temperature (T = 400 °C) leads to the formation of different kinds of oxynitride species, associated to a silicon-rich Si_3ON stoichiometry rather than the $SiNO_3$ observed for sample A. High temperature anneal (T = 700 °C), on the other hand, drastically decreases the oxygen content, thus resulting in a WER alignment for all the samples.

5. Conclusions

Amorphous SiNx:H thin films have been prepared using plasma-enhanced chemical vapor deposition using different process conditions to modulate film composition, chemical bonding, and chemical-physical properties. Samples have been characterized by X-Ray Photoelectron Spectroscopy (XPS), Fourier Transforms Infrared Spectroscopy (FT-IR), and X-ray diffraction (XRD). The wet etching behavior of the thin film in HF solution sheds light on the role of hydrogen percentage and oxygen contaminants on the chemical resistance of the amorphous layer.

The WER data can be rationalized in the following way.

- Sample A is the more etch-resistant layer mainly due to its low H content;
- Sample B is comparable to sample A, despite its higher H content: this similar behavior is due to its higher N/Si ratio and low Si-H bond density;
- Sample C is the less etch-resistant layer due to the highest H content, the lowest N/Si ratio, highest Si-H bond density.

Thickness reduction during etching is evaluated by straightforward methodology allowing to use of FT-IR spectral analysis without suffering the silicon substrate contributin (supplementary materials).

Annealing treatments causing a decrease of the oxygen in the layer as well as a transition toward the crystalline phase contribute to improving the resistance to acid attack. Obtained results confirm the presence of amorphous Si-O phase domains in the nitride networks and of Si-OH groups at the surface. Differences in oxygen content, due to adventitious contamination in the reactor, are responsible for the different WER of samples characterized by similar hydrogen content.

CRediT authorship contribution statement

Matteo Barcellona: Ivestigation, Validation, Formal analysis, Writing – original draft, Writing – review & editing. **Orazio Samperi:** Ivestigation, Validation, Formal analysis, Writing – original draft, Writing – review & editing. **Davide Russo:** Ivestigation, Validation, Formal analysis. **Anna Battaglia:** Resources. **Dirk Fischer:** Resources. **Maria Elena Fragalà:** Conceptualization, Supervision, Writing – original draft, Writing – review & editing.

Declaration of competing interest

The authors declare that they have no known competing financial interests or personal relationships that could have appeared to influence the work reported in this paper.

Data availability

Data will be made available on request.

Acknowledgments

Authors acknowledge Lam Research that provides stress and RBS-ERDA characterization of nitride layers and the Italian Ministry for Education, University and Research (MIUR) within the Bionanotech Research and Innovation Tower (BRIT) laboratory of University of Catania (Grant no. PONa3_00136) for the XRD and XPS facilities and SAMOTHRACE project for economical funding.

Appendix A. Supplementary data

Supplementary data to this article can be found online at https://doi.org/10.1016/j.matchemphys.2023.128023.

References

[1] M. Charles, Y. Baines, R. Bouis, A.M. Papon, Phys. Status Solidi 255 (2018), 1700406.
[2] C.H. Chang, H.T. Hsu, L.C. Huang, C.Y. Chiang, E.Y. Chang, Asia-pacific microwave conference proceedings, APMC (2012) 941–943.
[3] M.J. Tadjer, T.J. Anderson, T.I. Feygelson, K.D. Hobart, J.K. Hite, A.D. Koehler, V. D. Wheeler, B.B. Pate, C.R. Eddy, F.J. Kub, Phys. Status Solidi 213 (2016) 893–897.
[4] H. Seidel, L. Csepregi, A. Heuberger, H. Baumgärtel, J. Electrochem. Soc. 137 (1990) 3612–3626.
[5] F. Koehler, D.H. Triyoso, I. Hussain, S. Mutas, H. Bernhardt, IOP Conf. Ser. Mater. Sci. Eng. 41 (2012), 012006.
[6] F. Koehler, D.H. Triyoso, I. Hussain, B. Antonioli, K. Hempel, Phys. Status Solidi 11 (2014) 73–76.
[7] P. Muellner, E. Melnik, G. Koppitsch, J. Kraft, F. Schrank, R. Hainberger, Procedia Eng. 120 (2015) 578–581.
[8] M. Sagmeister, G. Koppitsch, P. Muellner, S. Nevlacsil, A. MaeseNovo, R. Hainberger, D. Seyringer, J. Kraft, Proc West Mark Ed Assoc Conf 2 (2018) 1023.
[9] V.G.T. Vangipuram, Journal of the Microelectronic Engineering Conference 25 (2019).
[10] U.K. Mishra, P. Parikh, Y.F. Wu, Proc. IEEE 90 (2002) 1022–1031.
[11] B.M. Green, K.K. Chu, E.M. Chumbes, J.A. Smart, J.R. Shealy, L.F. Eastman, IEEE Electron. Device Lett. 21 (2000) 268–270.
[12] T.L. Chu, J. Vac. Sci. Technol. 6 (2000) 25.
[13] K. Kijima, N. Setaka, H. Tanaka, J. Cryst. Growth 24–25 (1974) 183–187.
[14] A.E. Kaloyeros, Y. Pan, J. Goff, B. Arkles, ECS Journal of Solid State Science and Technology 9 (2020).
[15] C. Yang, J. Pham, Silicon 6 10 (2018) 2561–2567, 2018 10.
[16] H. Amjadi, IEEE Trans. Dielectr. Electr. Insul. 6 (1999) 852–857.
[17] T. Otani, M. Hirata, Thin Solid Films 442 (2003) 44–47.
[18] S.N. Hsiao, N. Britun, T.T.N. Nguyen, T. Tsutsumi, K. Ishikawa, M. Sekine, M. Hori, Plasma Process. Polym. 18 (2021).
[19] W. van Gelder, V.E. Hauser, J. Electrochem. Soc. 114 (1967) 869.
[20] J.F. Moulder, W.F. Stickle, P.E. Sobol, K.D. Bomben, Handbook of X-Ray Photoelectron Spectroscopy, 1992.
[21] Raymund W.M. Kwok, XPS Peak 4.1 (2000).
[22] I. Jonak-Auer, R. Meisels, F. Kuchar, Infrared Phys. Technol. 38 (1997) 223–226.
[23] W.A. Lanford, M.J. Rand, W.A. Lanford, M.J. Rand, JAPCA 49 (1978) 2473–2477.

[24] N. Hegedüs, K. Balázsi, C. Balázsi, Materials 14 (2021) 5658, 5658 14 (2021).
[25] G. Kissinger, D. Kot, I. Costina, M. Lisker, ECS Journal of Solid State Science and Technology 8 (2019) N125–N133.
[26] D.M. Knotter, J. Am. Chem. Soc. 122 (2000) 4345–4351.
[27] L. Tang, Y. Zhu, J. Yang, Y. Li, W. Zhou, J. Xie, Y. Liu, F. Yang, J. Semiconduct. 30 (2009), 096005.
[28] L.H. Liu, D.J. Michalak, T.P. Chopra, S.P. Pujari, W. Cabrera, D. Dick, J.F. Veyan, R. Hourani, M.D. Halls, H. Zuilhof, Y.J. Chabal, J. Phys. Condens. Matter 28 (2016), 094014.
[29] M.J. Helix, K.v. Vaidyanathan, B.G. Streetman, H.B. Dietrich, P.K. Chatterjee, Thin Solid Films 55 (1978) 143–148.
[30] C. Boehme, G. Lucovsky, J. Appl. Phys. 88 (2000) 6055–6059.
[31] J.A. Taylor, G.M. Lancaster, A. Ignatiev, J.W. Rabalais, J. Chem. Phys. 68 (2008) 1776.
[32] G.M. Ingo, N. Zacchetti, D. della Sala, C. Coluzza, J. Vac. Sci. Technol. A: Vacuum, Surfaces, and Films 7 (1998) 3048.
[33] P. Cova, S. Poulin, O. Grenier, R.A. Masut, J. Appl. Phys. 97 (2005), 073518.
[34] P. Mota-Santiago, A. Nadzri, F. Kremer, T. Bierschenk, C.E. Canto, M.D. Rodriguez, C. Notthoff, S. Mudie, P. Kluth, J. Phys. D Appl. Phys. 55 (2022), 145301.
[35] M. Matsuoka, S. Isotani, W. Sucasaire, L.S. Zambom, K. Ogata, Surf. Coat. Technol. 204 (2010) 2923–2927.
[36] S. Chopra, R.P. Gupta, S. Banerjee, J. Nanosci. Nanotechnol. 11 (2011) 11216–11221.
[37] S. Karthick, C. Elanchezhian, B.V. Ramnath, M. Saravanan, K. Giridharan, Biomass Convers Biorefin (2022).
[38] Y. Li, L. Wang, S. Yin, F. Yang, Mater. Chem. Phys. 141 (2013) 874–881.
[39] L.M. Loewenstein, C.M. Tipton, J. Electrochem. Soc. 138 (1991) 1389–1394.
[40] L. Tang, Y. Zhu, J. Yang, Y. Li, W. Zhou, J. Xie, Y. Liu, F. Yang, J. Semiconduct. 30 (2009), 096005.
[41] R. Chow, W.A. Lanford, W. Ke-Ming, R.S. Rosler, J. Appl. Phys. 53 (1998) 5630.
[42] J.S. Judge, J. Electrochem. Soc. 118 (1971) 1772.
[43] D. Watanabe, H. Aoki, M. Itano, T. Kezuka, C. Kimura, T. Sugino, Microelectron. Eng. 86 (2009) 2161–2164.